# Upper-Tropospheric Humidity from MLS and ECMWF Reanalyses

H. L. CLARK* AND R. S. HARWOOD

*Institute for Meteorology, University of Edinburgh, Edinburgh, United Kingdom*

(Manuscript received 31 October 2001, in final form 26 July 2002)

ABSTRACT

This paper compares upper-tropospheric humidity from the Microwave Limb Sounder (MLS) on the *Upper Atmosphere Research Satellite* with European Centre for Medium-Range Weather Forecasts (ECMWF) data. MLS measurements are not included in the ECMWF analyses, and so a comparison of two independent datasets is possible. The focus of this paper is on the tropical region from 1991 to 1997 when MLS measurements are available and, to be more specific, from 1991 to 1994 during the ECMWF 15-yr reanalysis period (ERA-15). It is found that the contrast between moist and dry areas, or areas of convection and subsidence, is less pronounced in ECMWF data than in MLS measurements. This result applies on the scale of both global and regional circulations and results in a semiannual cycle of high and low correlations between the two datasets that is particularly pronounced over South America. Time series show that the impact of model changes to the absolute values of humidity make long-term comparison with MLS difficult.

## 1. Introduction

Water vapor measurements in the upper troposphere are difficult to obtain. In situ measurements from radiosondes, balloons, and aircraft are limited in their spatial and global coverage. The radiosonde network has long provided the main source of water vapor observations, but radiosondes have limited accuracy in the upper troposphere (e.g., Elliot and Gaffen 1991; Soden and Lanzante 1996). Radiosonde profiles are confined largely to Northern Hemisphere landmasses with the result that the water vapor field in the upper troposphere, particularly in the tropical region, has been poorly observed. Satellites provide a greater spatial and temporal coverage. The Microwave Limb Sounder (MLS) on the *Upper Atmosphere Research Satellite* (*UARS*), which is sensitive to water vapor in the upper troposphere (Read et al. 1995), provided near-global measurements of water vapor from September 1991 to August 1999. It offers several advantages over other satellite instruments. MLS has a vertical resolution of about 3 km in contrast to infrared instruments such as Meteosat (Schmetz and Turpeinen 1988), the U.S. Geostationary Operational Environmental Satellite (GOES; Soden and Bretherton 1993), and the Television and Infrared Observation Satellite (TIROS) Operational Vertical Sounder (TOVS; Salathé and Chesters 1995), which are sensitive to water vapor in a broad layer of the upper troposphere about 300 hPa thick. The MLS measurement of upper-tropospheric humidity is relatively insensitive to cirrus clouds, giving it additional advantages over infrared techniques. The temporal resolution of MLS is better than that of solar occultation instruments such as the Stratospheric Aerosol and Gas Experiment 2 (SAGE II) from which measurements are limited to about 30 per day; MLS makes about 600 measurements per day in the tropical region.

Both satellite and in situ measurements have their advantages and weaknesses, and hence they are often combined or assimilated into a new dataset exploiting the positive aspects of both. Assessing the validity of the assimilated dataset is then difficult since all suitable measurements have gone into its production and hence there are no independent measurements with which it can be compared. The European Centre for Medium-Range Weather Forecasts (ECMWF) reanalysis (ERA-15) humidity fields assimilate data from both TOVS and the radiosonde network, and so the MLS dataset is useful for comparison with ERA since its observations are not included in the ERA assimilation. In this paper, we compare *UARS* MLS relative humidity observations at 215 hPa with ECMWF relative humidity data. As already stated, there are likely to be problems in both datasets: ECMWF suffers from a sparse input of data, and MLS has some technical difficulties measuring water vapor in this region [line-shape information cannot be used in the same way for upper-tropospheric measurements as for stratospheric measurements (Read et al. 2001)]. Because of this, we undertake a comparison

* Current affiliation: CNRM, Toulouse, France.

*Corresponding author address:* Hannah Clark, CNRM, 42 Ave. Gaspard Coriolis, 31057 Toulouse Cedex 1, France.
E-mail: hannah.clark@cnrm.meteo.fr

to cast light on the likely strengths and weaknesses of both datasets. The ECMWF data and MLS data are described in section 2. We discuss time series of tropical mean values in section 3 and the spatial differences between the two fields in section 4, summarizing our conclusions in section 5.

## 2. Data

### *a. ECMWF humidity analysis*

Details of the ECMWF 15-yr reanalysis project can be found in Gibson et al. (1997). Over most areas of the globe, there are insufficient observations to support the analysis with the required accuracy. In regions for which the data are sparse, the analysis relies upon satellite-based observations. The data assimilation scheme that is used to produce ERA makes use of the ECMWF numerical forecast model to infer information about the state of the atmosphere from data-rich areas to data-sparse areas. Output from the ECMWF forecast model is combined with observations and forcing fields to form the input for the analysis. Results from the analysis, after initialization, are used as initial conditions for the next forecast, and this process is repeated.

The ECMWF analysis assimilates observations from the TOVS satellite and from radiosondes. TOVS consists of three passive vertical sounding instruments, the High Resolution Infrared Radiation Sounder (HIRS-2), the Microwave Sounding Unit, and the Stratospheric Sounding Unit (Smith et al. 1979). HIRS-2 is a radiometer with 19 channels in the infrared and 1 channel in the visible. HIRS channels 10, 11, and 12 are known as the ''water vapor channels'' because variations in humidity strongly affect the measured radiances. The Microwave Sounding Unit has four channels at around 55 GHz, and the Stratospheric Sounding Unit is an infrared radiometer with three channels near 15 $\mu$m. Cloud-cleared TOVS radiances were produced by the National Environmental Satellite, Data, and Information Service. The method of one-dimensional variational data assimilation (1DVar; Eyre et al. 1993; McNally and Vespirini 1996) is first used to obtain the atmospheric temperature and humidity profiles that best fit the radiances measured from these channels. The 1DVar temperature retrievals are used globally, over sea areas only, and below 100 hPa. Humidity retrievals from the water vapor channels are used below 300 hPa, over the seas only, and in the Tropics; only the cloud-free profiles are assimilated.

Radiosonde observations of humidity from below 300 hPa are used in the assimilation, but they are not considered to be accurate enough at the low temperatures and humidities above this height. Hence, above 300 hPa there is no assimilation of water vapor measurements and the analysis is based entirely on 1DVar. In this paper we assess how well the ERA data represent those from MLS at 215 hPa, above the 300-hPa cutoff. We focus primarily on a part of the 15-yr reanalysis data that overlaps with MLS, although some operational data will also be used. The changes to the analysis throughout the operational period will be described where appropriate.

### *b. MLS data*

*UARS*, described in Reber (1993), is in an almost circular orbit at an altitude of 585 km and an inclination of 57° to the equator. It makes about 15 orbits a day. MLS makes a limb scan perpendicular to the *UARS* orbit path from a tangent height of 90 km to the surface and provides a 3-km field of view in the vertical direction. The measurements of limb radiance from one scan are used to deduce profiles of temperature and of the mixing ratio of various species, with the profiles being retrieved onto a fixed pressure grid. MLS has two viewing directions. It looks from 80°N to 34°S for about 36 days and then executes a yaw maneuver to look from 34°N to 80°S for another 36 days or so. The tropical region is thus, barring occasional problems with the instrument, observed daily, and measurements are available from 19 September 1991 to August 1999. The MLS instrument is described in more detail by Barath et al. (1993), and the measurement technique is described by Waters (1993).

The 205-GHz channel on MLS is principally used to measure chlorine monoxide, but it is sensitive to water vapor in the upper troposphere when concentrations are in the range of 100–300 ppmv (Read et al. 1995). Since the initial retrieval described in Read et al. (1995), there have been a further two versions released, version 490 (V490) and version 5 (V5), both of which used an improved forward model and a nonlinear least squares retrieval constrained by a priori estimates. Full details of the retrievals are described in Read et al. (2001). The two more recent versions are drier than the initial version by about 60–70 ppmv (Sandor et al. 1998) but are qualitatively similar. The excess humidity in the initial version was caused by an error in the dry continuum absorption coefficient, which was determined from stratospheric radiances and did not extrapolate well into the upper troposphere. Both V490 and V5 used tropospheric radiances to determine the dry and wet absorption coefficient functions.

The main difference between V490 and V5 comes from the determination of the wet component of the absorption coefficient. In V490, the absorption coefficients were calculated from radiances in what is believed to be saturated air, and there was an assumed insensitivity to ice emissions. For version 5, however, absorption coefficients were calculated using coincident Vaisala, Inc., radiosonde measurements. More details about the the V490 and V5 measurements can be found in Read et al. (2001) and Livesey et al. (2002). Although the retrieval was performed in relative humidity with respect to ice (RHi), the standard V5 level-3at files con-

tain volume mixing ratios that were converted from RHi using National Centers for Environmental Prediction (NCEP) temperatures. We investigate both of these quantities.

Retrievals in the upper troposphere may be affected by thick cirrus clouds. In the tropical region between 6 and 12 km the retrievals are not significantly affected, but at latitudes poleward of 40° a significant fraction of the measured radiances may come from scattering by cirrus clouds (Bond 1996). Ice crystals in cirrus clouds at a concentration of 0.1 g $m^{-3}$ over a horizontal distance of 120 km could contribute to about 20% of the absorption coefficient at 215 hPa but will usually be less, and at concentrations of less than 0.01 g $m^{-3}$ the effect is negligible (Read et al. 1995). Ice crystal concentrations of 1 g $m^{-3}$ will emit 20 times as much radiation at 203 GHz than will vapor at 100% RHi. For cirrus associated with a major convective system, such values are not uncommon and have been seen in MLS data. Cirrus that are not associated with convective systems typically have concentrations of 0.003 g $m^{-3}$ or less (Knollenberg et al. 1993) and contribute an equivalent of 6% RHi. Since there is expected to be a 20% uncertainty in the continuum functions, thin cirrus clouds are not expected to contribute significantly to MLS upper-tropospheric humidity (UTH) errors (Read et al. 2001). Values of relative humidity greater than 120% are assumed to be indicative of ice contamination and are reset to 100% in this study as advised in Read et al. (2001).

## 3. Time series of tropical mean values

### *a. Relative humidity*

Figure 1 shows a time series of MLS relative humidity between 30°N and 30°S. To reduce any sampling differences with ECMWF, the data were zonally averaged and the resulting averages were area weighted by the cosine of their latitude. As MLS has aged, it has operated more intermittently. Measurements were made until June 1999 but with an increasing number of missing days. We have less confidence in the MLS data after 15 June 1997 when the 63-GHz radiometer was switched off and changes to the scan pattern were made to conserve spacecraft power (Livesey et al. 2002). Figure 1a shows the raw data from MLS. The mean of the raw MLS data is 40.3%, with a variance of 7.7%. The variability is made up of natural variability of the atmosphere, random instrument noise, and an instrumental artifact associated with the yaw cycle.

The influence of the yaw cycle on the relative humidity measurements is shown in Fig. 1b, which shows an enlarged section of the time series, chosen to illustrate yaw cycles for which the effect is particularly clear. As the ends of a yaw cycle are approached, the antenna receives more radiation from the sun and becomes warmer, affecting the measured radiances. Figure 1c shows the change in antenna temperature over several yaw cycles. The increase in antenna temperature can be misinterpreted as a variation in water vapor (at 215 hPa it causes a reduction), as Fig. 1b reveals. The exact explanation for this is complicated. The antenna temperature varies by about 0.8 K over a yaw cycle and the retrieved relative humidities w.r.t. ice by about 7% (Read et al. 2001). The problem is greater in version 5 than in the previous two versions, is worse at 147 hPa (not used in this study) than at 215 hPa, and is more evident in mixing ratio than in relative humidity.

We make a linear correction for the yaw cycle based on the 0.8-K variation in antenna temperature and apply this to the raw data. The success of this yaw correction is illustrated in Fig. 1d. The removal of the yaw cycle reduces the variance of this short section of the time series from 6.3% to 4.7%. The variance in Fig. 1d is bigger than the precision of the measurements, estimated at 0.6% RHi for this area average. Some of this difference can be attributed to the day-to-day variability of the water vapor field and some to remaining variation over the yaw cycle, which has not been removed using the simple linear approximation. The yaw correction was applied to the whole time series, and the results are plotted in Fig. 1e. This reduces the variance of the time series from 7.7% to 5.8% but the mean is hardly affected. Corrections for the yaw effect are applied throughout the paper.

We account for any difference resulting from the different vertical resolution of the two datasets by multiplying vertical profiles of ECMWF relative humidities by the MLS averaging kernels in eight latitude bands ($-70°$, $-50°$, . . . , 70°). The averaging kernels for MLS are plotted in Read et al. (2001). The effect of multiplying the ECMWF relative humidities by the averaging kernels is small and relatively insignificant when compared with other effects, as we shall see later.

Figure 2 shows a time series of all MLS data between 30°N and 30°S with the corresponding ECMWF data, including both the reanalysis and the operational data. ECMWF is the initialized data, which have had gravity waves suppressed. As before, the data were zonally averaged first to reduce any sampling discrepancy between MLS and ECMWF, and the resulting averages were area weighted by the cosine of their latitude.

ERA-15 spans January 1979–February 1994 and provides time series of consistent meteorological analyses derived from a single version of the ECMWF model. From then on, comparisons with MLS are more difficult. The ECMWF analyses enter a pre-reanalysis mode before switching to the operational analysis on 4 April 1995. The operational analyses are subject to a wide range of different changes that may or may not have affected the water vapor field, and we illustrate a few here that we imagine to be the most significant. For easy comparison, the time series are plotted as the variation about the mean, scaled by the mean. Absolute values are indicated on the right-hand axes. Figure 2a shows

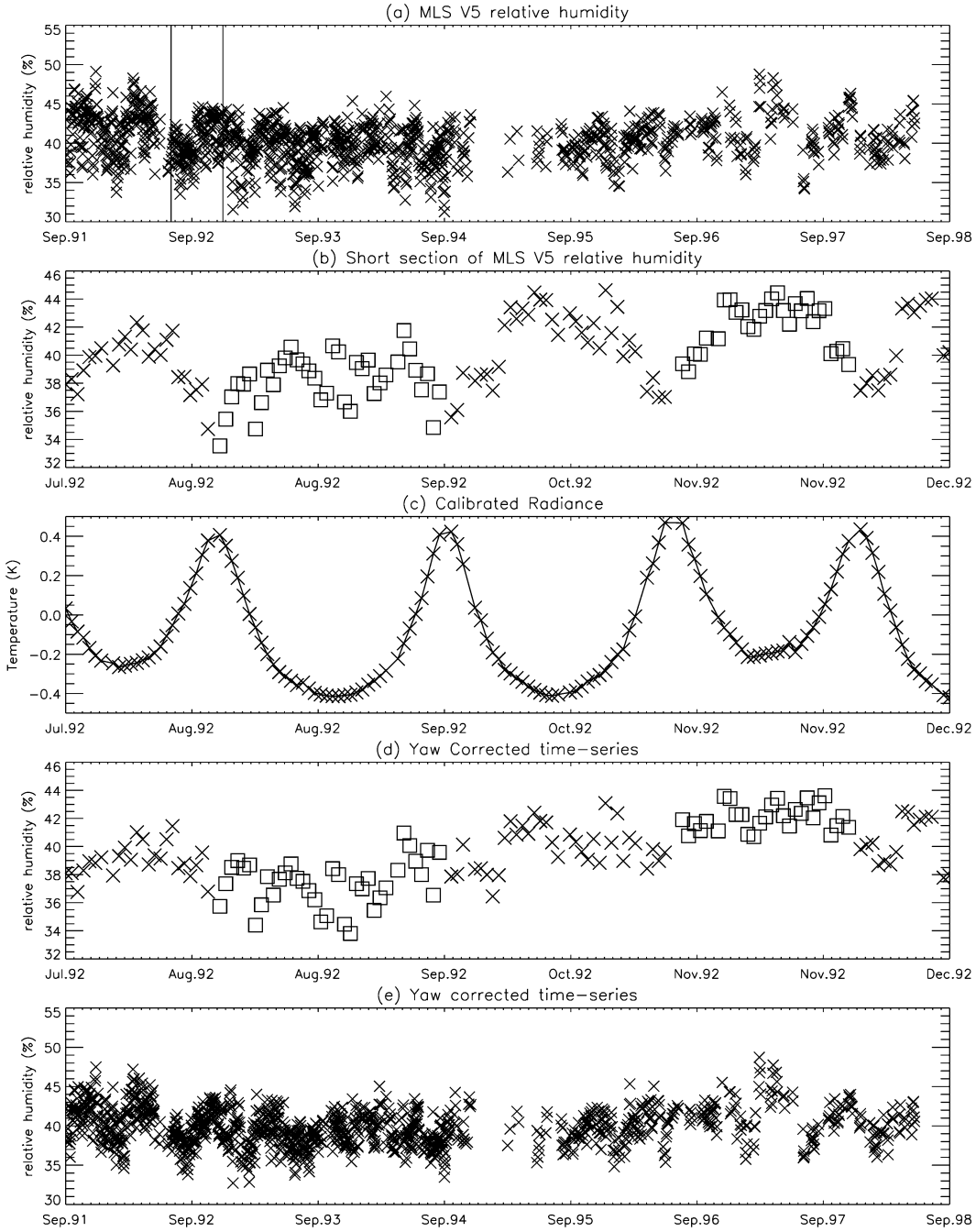


FIG. 1. (a) Time series of raw MLS, version-5, 30°N–30°S averaged relative humidity measurements. (b) Subset of time series: Vertical lines in (a) indicate the region that has been expanded. (c) The change in calibrated radiance over a yaw cycle. (d) Yaw-corrected version of (b). (e) The yaw correction applied to the whole time series in (a). In (b) and (d), the crosses represent north-looking days and the squares are for south-looking days.

the MLS relative humidity data after the yaw cycle has been removed as just discussed. Figure 2b shows the ECMWF relative humidities. The mean of the ECMWF relative humidity time series is 41.4%, with a variance of 17.7%. The variance is much larger than for MLS, because the ECMWF analyses scheme has been subjected to a number of changes over this period.

The most obvious discontinuity in the ECMWF time series takes place at the end of the ERA period in 1994 (marked as ''end era'' in Fig. 2c), when the analysis reverted to the mode that was operational in the period before ERA. The ERA system became operational on 4 April 1995 (marked as ''end pre-era''). The 3D variational data assimilation analysis (Courtier et al. 1998)

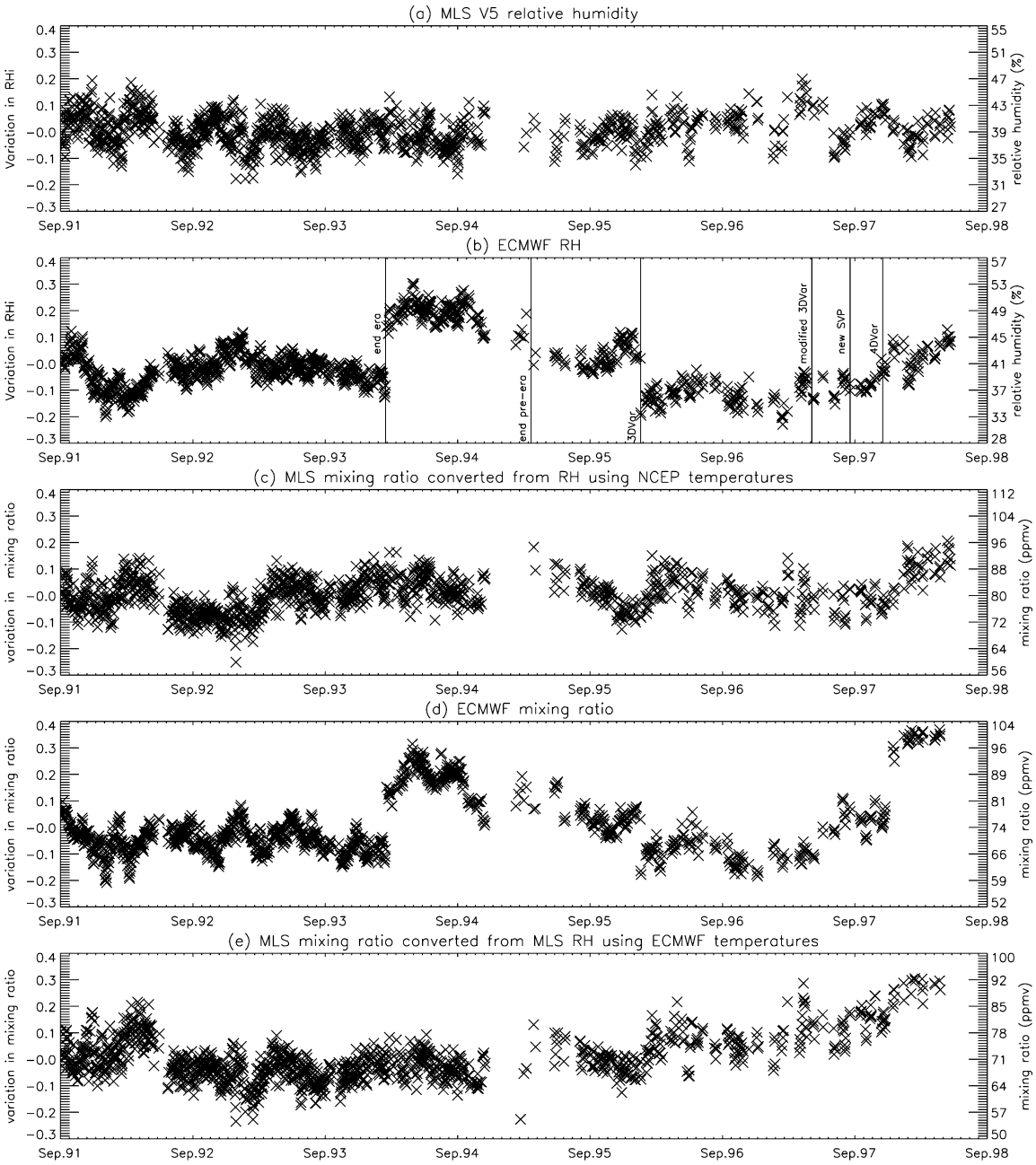


FIG. 2. Time series of 30°N and 30°S averaged water vapor: (a) MLS RHi with the yaw cycle removed (see Fig. 1), (b) the equivalent days from ECMWF RHi showing changes to the ECMWF analysis scheme, (c) MLS mixing ratios formed using the NCEP temperatures, (d) ECMWF mixing ratios formed from ECMWF temperatures, and (e) MLS mixing ratios formed from ECMWF temperatures. Left-hand axes are plotted as variation from the mean and are scaled by the mean. Right-hand axes give approximate absolute values.

was introduced on 30 January 1996 and is marked by the vertical line ''3DVar'' in Fig. 2c. Its subsequent modification is also marked. This was followed by the introduction of 4D variational data assimilation (''4DVar''; Rabier et al. 1998) and by a new version of the Tetens formula to calculate saturation vapor pressure (''new SVP''). The variational analysis code was brought into line with the model, using saturation vapor pressure over water for temperatures above 0°C and over ice for temperatures lower than −23°C, and a mixed phase relationship between these two temperatures. Prior to this, the variational analysis code used saturation vapor pressure over ice at temperatures lower than 0°C and over water at temperatures greater than 0°C. The new version of the Tetens formula to calculate saturation vapor pressure was seen to have a significant moistening effect on stratospheric humidity (Simmons et al. 1999).

The incorporation of 3D- or 4DVar is important be-

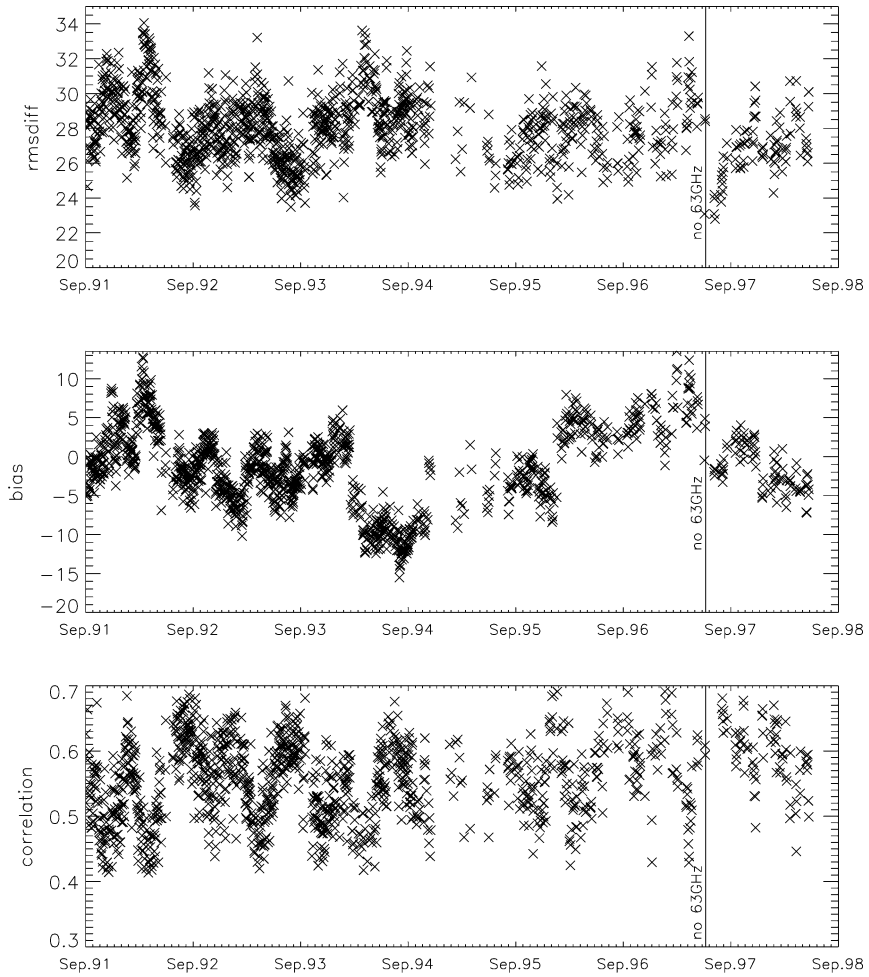


FIG. 3. Time series of daily (top) rms difference, (middle) bias, and (bottom) correlation for MLS and ECMWF relative humidity in the 30°N–30°S region.

cause the analysis of water vapor above 300 hPa contains no direct observations of water vapor and is based entirely on the 1D-, 3D-, or 4DVar scheme employed. In the stratosphere, the introduction of 3DVar caused a drifting toward unrealistically moist values (Simmons et al. 1999). In the upper troposphere, 3DVar caused a dramatic drop in relative humidity. The introduction of 4DVar, on the other hand, led to a gradual increase of relative humidity. Rabier et al. (1998) noted that equatorial averages of humidity for a test period in August 1995 were moister under the 4DVar scheme.

Figure 2e reveals an apparent drop in mixing ratio during boreal summer of 1992, with mixing ratios in the second half of 1992 being lower than those in the first half of the year. The drop is also seen in the mixing ratio converted using NCEP temperatures (Fig. 2c). We believe the drop to be real and suggest that it may be due to natural interannual variability such as ENSO, which is known to affect upper-tropospheric water from MLS (Newell et al. 1997; Chandra et al. 1998) and which led to enhanced moistening during the event of boreal winter 1991/92 (Waters et al. 1999).

Figure 3 shows the rms difference, the bias (MLS − ECMWF), and the correlation calculated for each day of the time series. The correlation here is between an MLS footprint and the interpolated value from the corresponding ECMWF analysis. It is therefore a measure of the daily spatial correlation between the two fields. This should be independent of any change in bias or linear gain produced by the retrieval or analysis system. We see that the rms difference is generally around 28% RHi. The bias drops by about 7% RHi at the time when the ECMWF analyses revert to their pre-era mode, and both the bias and the rms difference drop after 16 June 1997 when the 63-GHz radiometer was switched off and the scan pattern was changed to conserve power. The MLS retrieval became drier, but the data remained physically reasonable (Livesey et al. 2002) as is evidenced by the correlation coefficient, which does not show any dramatic change. The correlation coefficient

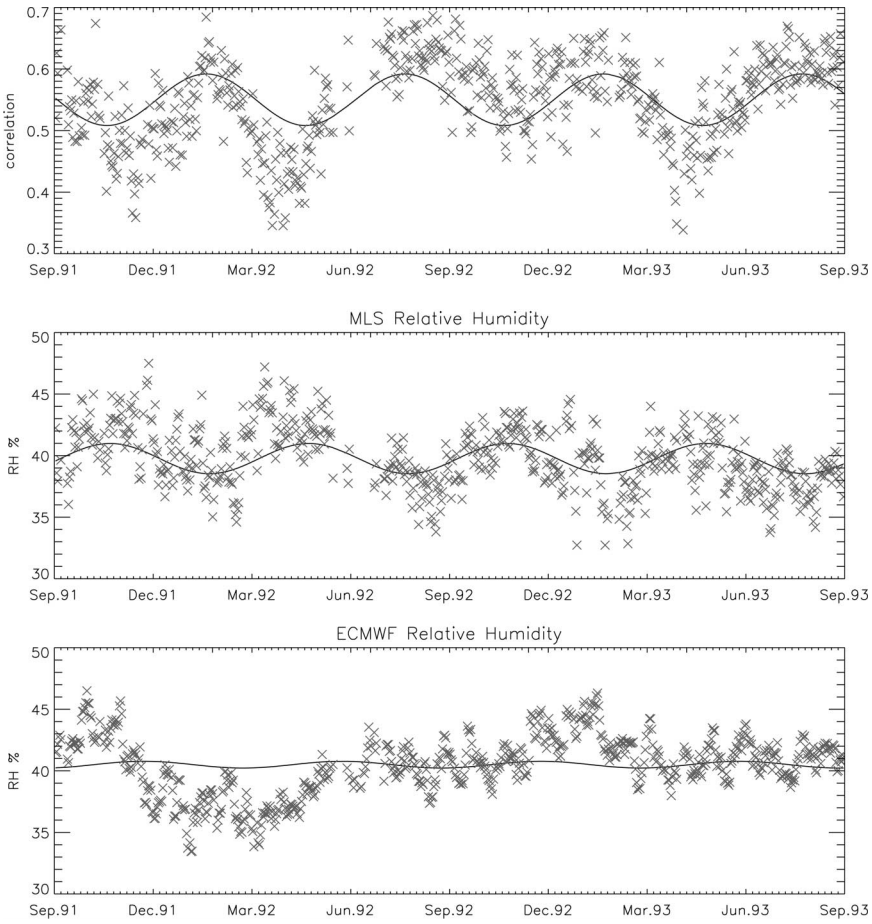


FIG. 4. (top) The spatial correlation between MLS and ECMWF RHi in the region 30°N–30°S, over the reanalysis period. A semiannual cycle has been fitted. The 30°N–30°S averaged (middle) MLS and (bottom) ECMWF RHi data with the same semiannual fit are also shown.

ranges from low (0.41) to moderate (0.69), with an average of 0.53. It may be that higher correlations would be achieved if the interpolated ECMWF values were based on more frequent analyses than every 6 h, but our investigations of the importance of diurnal variations suggest that this effect is small.

Note that the correlation coefficient is not affected by changes to the ECMWF analysis scheme, suggesting that the geographical features of the field are preserved and that it is only the bias between the two datasets that changes. The comparative poorness of the correlation indicates that one or the other of the two datasets would be unreliable for use in detailed climatological studies, and so we look further at the correlation to clarify their relative strengths and weaknesses.

Closer examination of Fig. 3 reveals that the correlation coefficient exhibits a semiannual oscillation. Figure 4 shows the correlation over the reanalysis period only, along with the MLS and ERA data, to which the same semiannual cycle has been fitted. The highest correlations are found in February and August. In the Northern Hemisphere, the semiannual oscillation in 300-hPa temperature has its maxima in April–May and October–November and thus coincides with the minimum correlations seen in Fig. 4. The highest correlations are found when the highest water vapor values have their most extreme displacement from the equator (Wu et al. 1993; Elson et al. 1996). The semiannual oscillation is strongly evident in the correlation coefficient and MLS values (Fig. 4, middle panel) but not in ERA data (Fig. 4, bottom panel). This suggests that some semiannual pattern is observed by MLS that is not captured by the ECMWF analysis.

A semiannual oscillation has been previously noted in MLS RHi and MLS mixing ratio fields (Newell et al. 1997; Sandor et al. 1998) and is evident in regions in which the intertropical convergence zone (ITCZ) crosses the equator two times per year (van Loon and Jenne 1970). Newell et al. (1997) found that the semiannual component was largest over land, extending into the Atlantic northeastward from Brazil. The discrepancy of the two fields may be due to a mismatch in convection over the landmasses or to differences in the position of the ITCZ. Figure 5 shows examples of the two fields at

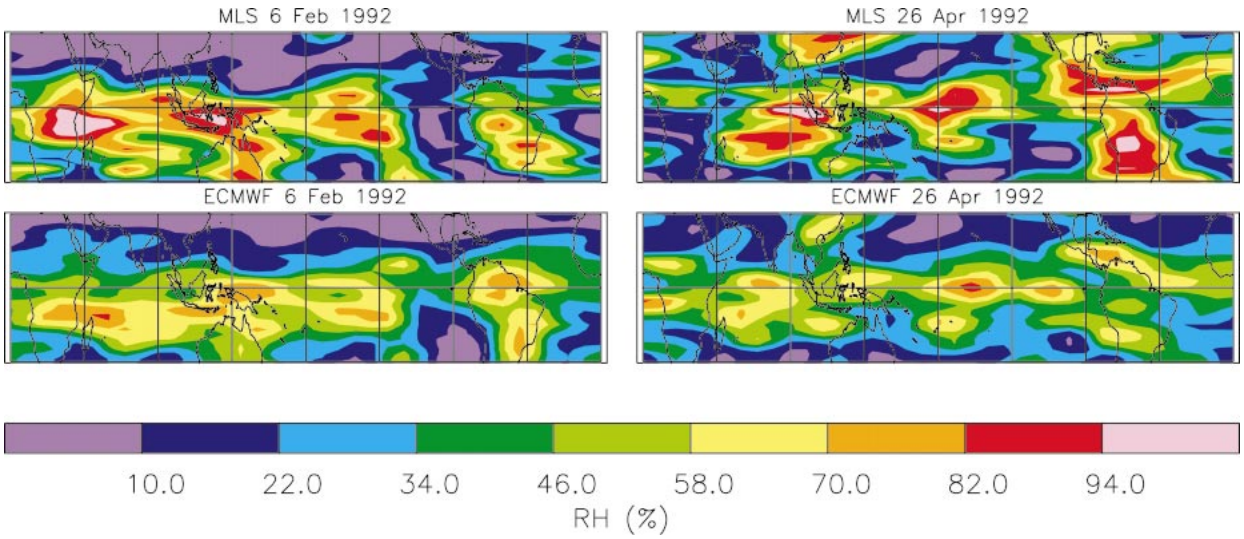


FIG. 5. Days with above-average (6 Feb 1992) and below-average (26 Apr 1992) correlation between (top) MLS and (bottom) ECMWF fields. Correlations are 0.68 and 0.46, respectively.

high and low correlation, namely, 6 February 1992 and 26 April 1992, respectively. For 6 February the similarity between the two fields is obvious, but for 26 April there are some large discrepancies. The MLS field (Fig. 5, top) has a region of enhanced moisture over South America that is absent in the ECMWF field. Likewise, MLS shows a region of increased moisture over China and Indonesia that is not revealed by ECMWF. We discuss the difference between the two fields in greater detail in section 4.

### *b. Mixing ratio*

We now describe some of the differences between the MLS and ECMWF fields that are evident when the relative humidities are converted to mixing ratios. Mixing ratios are converted from RHi using the Clausius–Clapeyron equation.

Figure 2c shows MLS mixing ratios calculated using MLS RHi and the NCEP temperatures, which give rise to the mixing ratio fields from the standard V5 level-3at files. Figure 2d shows ECMWF mixing ratios calculated from ECMWF RHi and ECMWF temperatures, and Fig. 2e shows mixing ratios from MLS relative humidity and ECMWF temperatures. ECMWF temperatures are linearly interpolated onto 215 hPa to be consistent with the use of NCEP temperatures in the operational production of the MLS level-3at files. We can see from this figure that the different temperature fields have a big impact on the deduced mixing ratios.

First, there is a difference in the mean values between Figs. 2c and 2d, which show the MLS–NCEP mixing ratios and the ECMWF mixing ratios, respectively. The MLS–NCEP ratio has a mean of 80 ppmv, and ECMWF has a mean of 74 ppmv. The mean mixing ratio of MLS–NCEP is reduced when ECMWF temperatures are used to create the mixing ratios from MLS RHi, and they become comparable in value to those from ECMWF.

Second, we see that the use of different temperature fields has altered the variability of the fields about the mean. The RHi time series from MLS shown in Fig. 2a has much less variability than either of the two mixing ratio fields calculated from it (Figs. 2c and 2e). The scaled variance (variance/mean) is 0.14 in Fig. 2a as compared with 0.34 in Fig. 2c and 0.49 in Fig. 2e. Comparison of Figs. 2d and 2e, however, shows that not all of the variability comes from the temperature field employed, since the temperatures are the same in both of these cases but the variability in Fig. 2d, the ECMWF–ECMWF case, is higher (0.91) than that of MLS–ECMWF (0.49).

Thus, the resulting mixing ratios are dependent on the quality of the temperature analyses. These are discussed by Trenberth et al. (2001). The NCEP and ECMWF temperature fields are not entirely independent, since both fields include brightness temperatures from the Microwave Sounding Unit (MSU). However the MSU temperatures have a stronger influence on the NCEP temperatures than on the ERA temperatures, because the ERA temperatures are influenced more strongly by HIRS.

MLS mixing ratio fields calculated using both NCEP and ECMWF temperatures show more variability than the MLS relative humidity. This leads us to consider to what extent the information comes from the MLS retrieval and to what extent it is dependent on the temperature used. The retrieval process requires temperatures in several places. It is found (Read et al. 2001; W. G. Read 2002, personal communication) that the relative humidity values are insensitive to the adopted temperatures (less so than would be the case for direct retrieval in terms of mixing ratio). The reason is a nonobvious

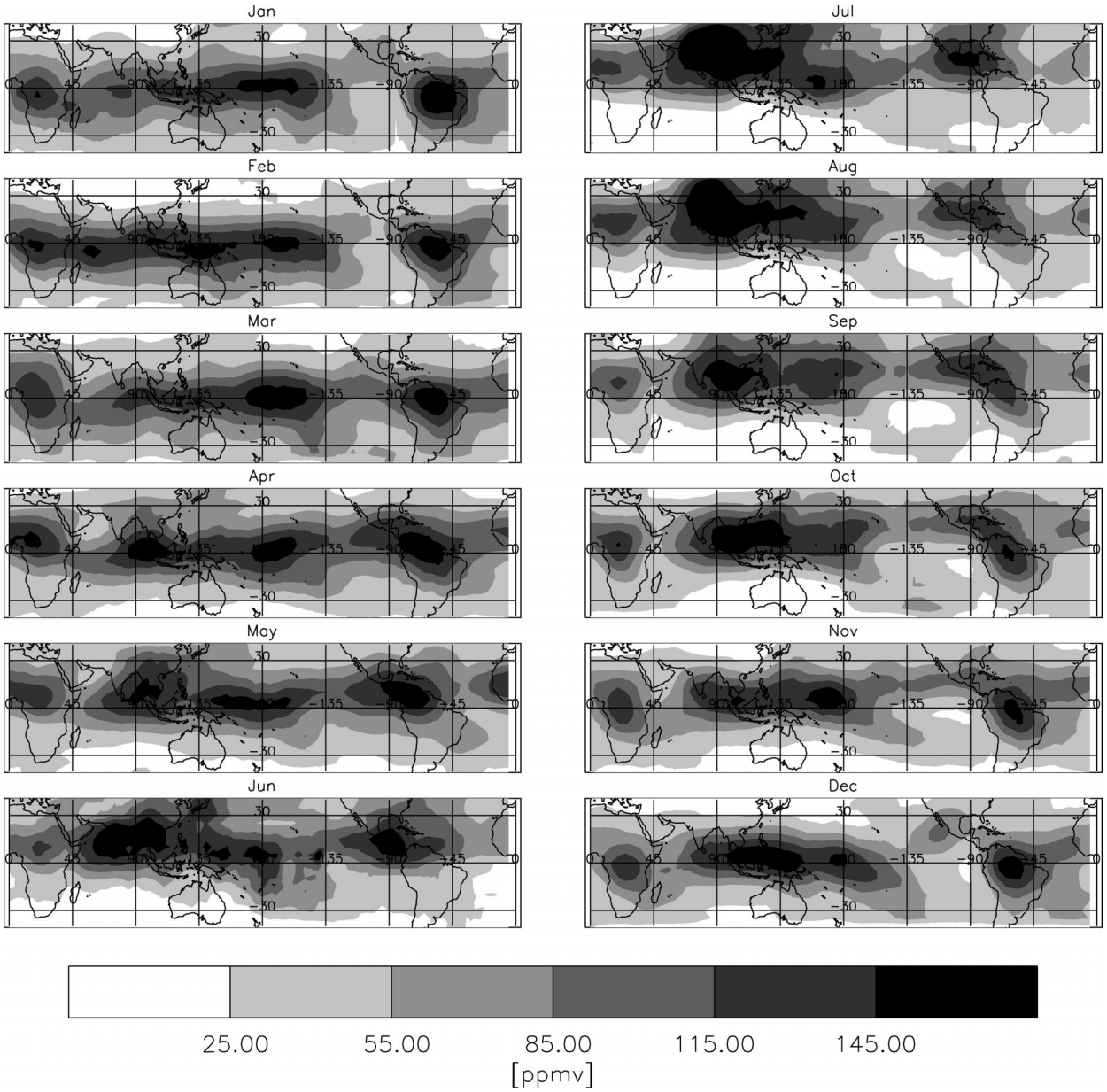


FIG. 6. Monthly averaged MLS mixing ratio (ppmv) at 215 hPa for Jan–Dec 1992. Mixing ratios have been produced from relative humidity using the ECMWF temperatures.

cancellation between the effects of the dependence of saturation mixing ratio on temperature and the effects of the temperature dependence of other parameters in the retrieval, such as the wet and dry continuum absorption coefficients.

We continue to describe the differences between MLS and ECMWF in terms of mixing ratio that has been calculated from relative humidity using the ECMWF temperature fields. Although this means that the two fields are not totally independent, any differences between them must be due to the differences in the relative humidity fields rather than to the temperature fields.

## 4. Spatial variations

This section examines the spatial differences between the two water vapor fields. Monthly averages of mixing ratio for MLS and ECMWF are plotted in Figs. 6 and 7, respectively. MLS and ECMWF data have both been averaged into 5° by 5° bins. Figure 8 shows the difference between MLS and ECMWF monthly means (i.e., Fig. 6 minus Fig. 7). As stated previously, any differences must result from differences in the relative humidity field, since the temperatures are the same in both cases.

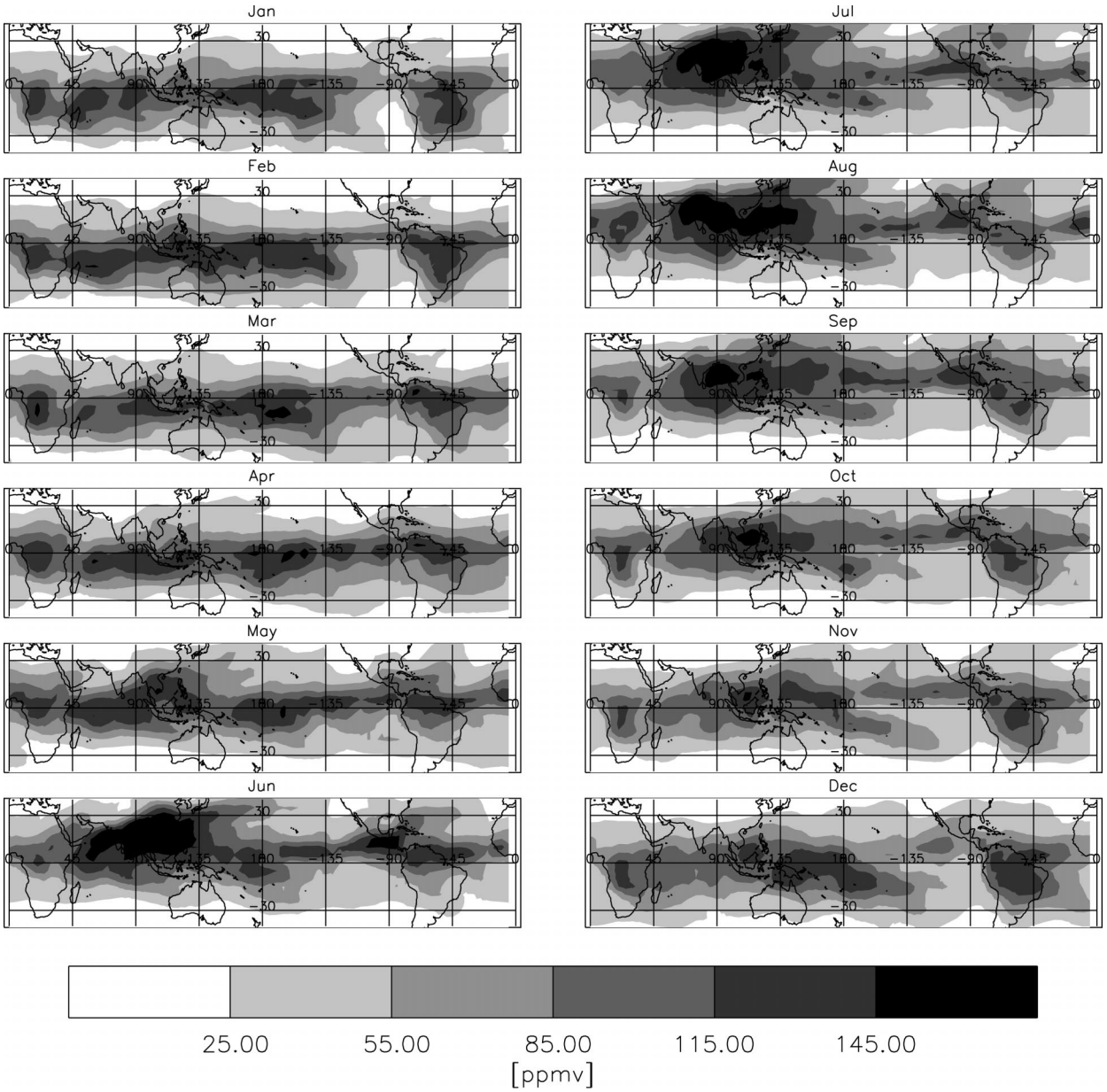


FIG. 7. Monthly averaged ECMWF mixing ratio (ppmv) at 215 hPa for Jan–Dec 1992. ECMWF relative humidities were multiplied by the MLS vertical averaging kernel, and ECMWF temperatures were used in conversion to mixing ratio as in Fig. 6.

*a. ITCZ and SPCZ*

The effects of the Hadley circulation upon upper-tropospheric moisture have been widely noted and lead to higher mixing ratios in the Tropics than in the subtropics. The large-scale ascent within the Hadley circulation is marked by a narrow band of deep cumulus convection that extends across the Tropics as the ITCZ. This is well pronounced in Figs. 6 and 7 as a band of water vapor mixing ratios of 85–115 ppmv lying just north or south of the equator.

In the eastern Pacific and Atlantic Oceans, the ITCZ is located mostly north of the equator at all times of the year. Its most northerly position is about 10°N in June–December in the Pacific, and it lies along the equator in March and April. Over the Indian Ocean, the ITCZ is less pronounced as a narrow band. From January to April, the higher mixing ratios are found in the Southern Hemisphere, extending to about 15°S. During Northern Hemisphere summer, high mixing ratios extend to about 5°S and in the Northern Hemisphere merge into the Asian monsoon region.

For most of the year, the difference plot, Fig. 8, shows two parallel bands lying north and south of the equator in the central and eastern Pacific, where MLS shows

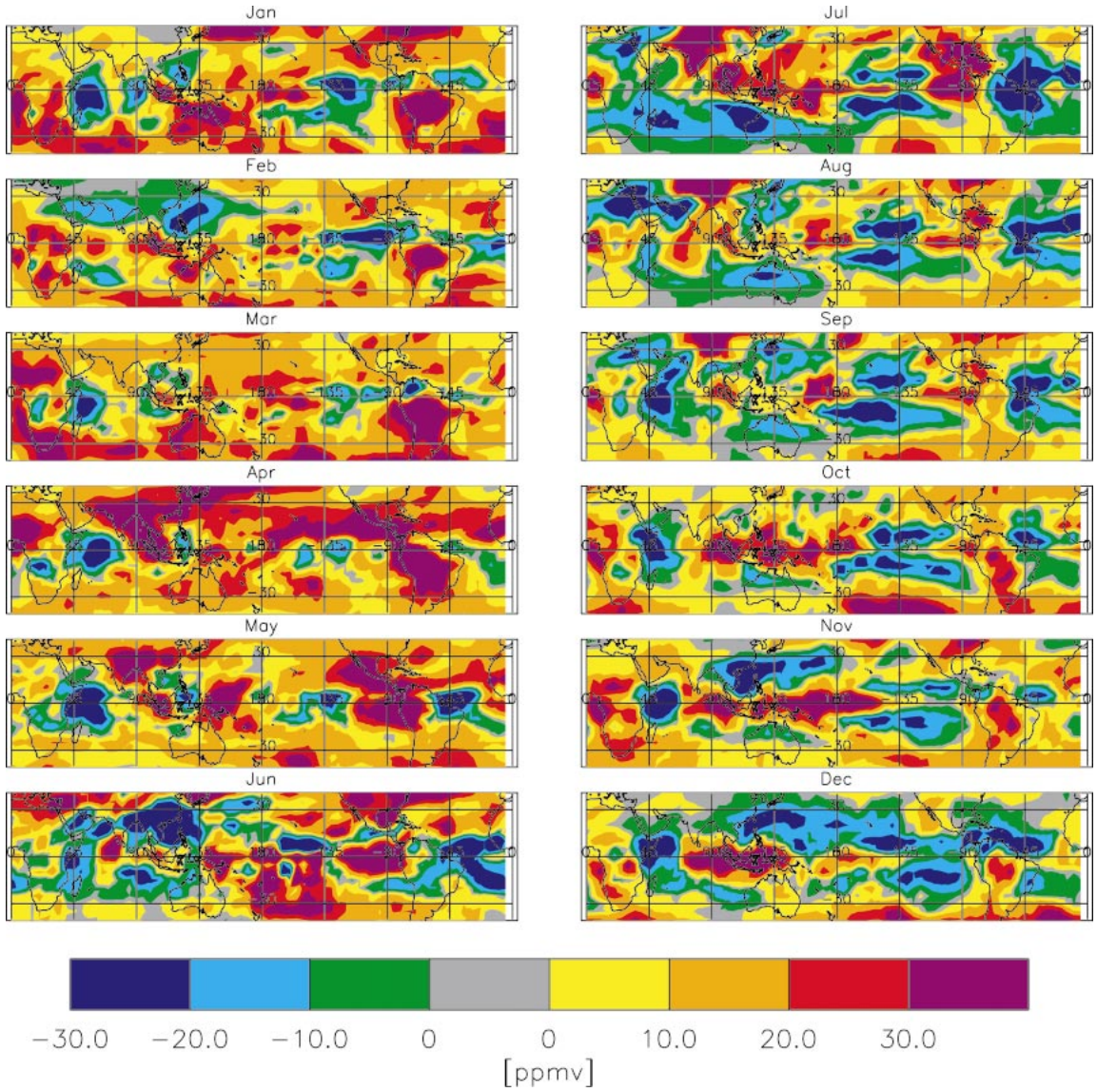


FIG. 8. MLS minus ECMWF monthly averaged mixing ratio (ppmv) at 215 hPa for Jan–Dec 1992.

much drier air than ECMWF does. This could result from the ECMWF analyses underestimating the dryness of the descending branch of the Hadley circulation, a feature that has been noted in several previous studies (e.g., Soden and Bretherton 1994; Schmetz and van der Berg 1994; Salathé and Chesters 1995) and that may contribute to the semiannual cycle in the correlation coefficient seen in Fig. 4.

The ITCZ in the Pacific is split into a northern component and a southern component known as the South Pacific convergence zone (SPCZ). The SPCZ is evident as a band of high mixing ratios extending in a southeasterly direction from New Guinea to about 225°E. The SPCZ appears more distinct from the ITCZ in ECMWF data than in MLS data. This may be due to a greater degree of moistening over the warm-pool region, which obscures the boundary between the ITCZ and SPCZ in MLS data, and to the reduced horizontal resolution of MLS data as compared with ECMWF.

The position and strength of the SPCZ is known to vary seasonally, being most pronounced from December to February and least pronounced between June and August, and it also varies on interannual and intraseasonal timescales (e.g., Vincent 1994). The seasonal variation in position of the SPCZ is exhibited in both MLS and ECMWF datasets. In MLS data, the SPCZ is well marked from October to March, achieving its most eastward extent to 135°W or 225°E. By comparison, in June–July–August (JJA) the SPCZ extends to about 200°E. The seasonal variation in the strength of the SPCZ seems to be less well captured by ECMWF, which shows it to be pronounced all year. Its easterly extent,

however, shows a similar variation to that of MLS. This tendency for the SPCZ to be a more persistent and well-marked feature in the ECMWF model has been noted by Vespirini (1998). Newman et al. (2000) however compared ERA data with outgoing longwave radiation (OLR), precipitation, and 200-hPa wind divergence from both observations and from two other reanalysis datasets, that of NCEP and that of the National Aeronautics and Space Administration Goddard Laboratory for Atmospheres. They argued that a double ITCZ was not a feature in the ECMWF fields and that ECMWF compared well with the observations of OLR and precipitation.

High mixing ratios are seen off the coast of Panama during June and July and are replaced from October to March by lower mixing ratios that extend along the coast of South America. This band of dry air lies between the coast of South America and the SPCZ. In both the MLS (Fig. 6) and ECMWF (Fig. 7) fields, it is a strong feature from September to February when the SPCZ is also strong and the dry band is flanked by moist air. From March to August, the dry band and the moist SPCZ are both weaker features. The dry band, as with the SPCZ, is more persistent in the ECMWF data, being evident during northern summer, too. This persistence was noted by Vespirini (1998), who attributed it to biased data rather than to a shortcoming of the model. Between August and February, the dry tongue is shown to be moister in ECMWF than in MLS (Fig. 8). An overestimation of humidity by the ECMWF model in this region was reported by Vespirini (1998) and Soden and Bretherton (1994) when they compared ECMWF data with data from the Special Sensor Microwave Imager (SSM/I). Soden and Bretherton noted that the assimilation of TOVS retrievals in this region may contribute to the problem because a moist bias arises from TOVS total precipitable water content through errors in the cloud clearance method.

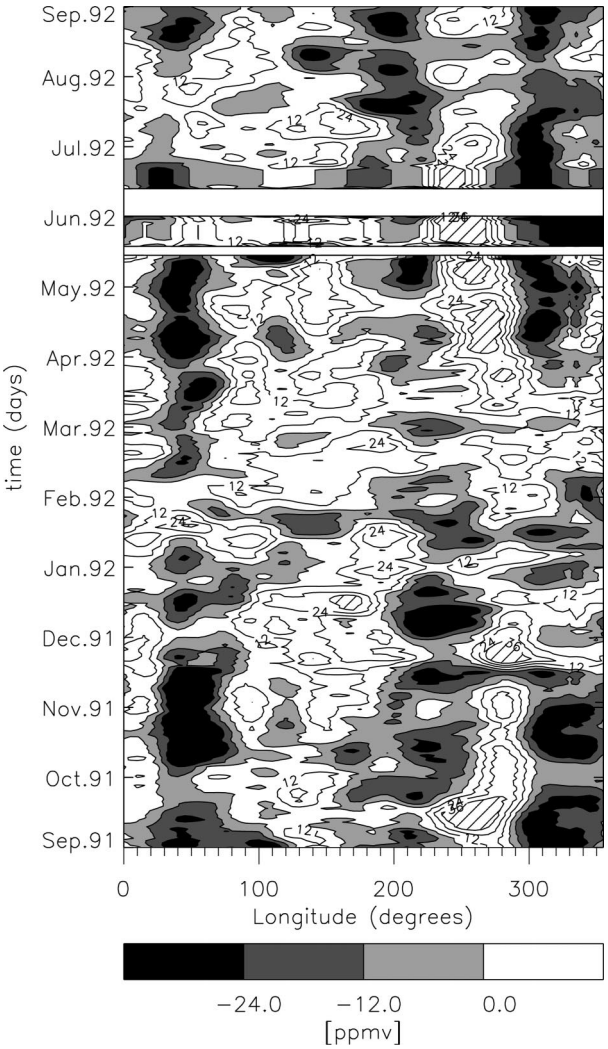


FIG. 9. Longitude–time diagram showing the difference (MLS − ECMWF) in mixing ratio at the equator and 215 hPa. Contour interval is every 12 ppmv, with values less than 0 shaded and values greater than 36 ppmv hatched.

### *b. Continental centers*

There are notable regions of high water vapor mixing ratios that coincide with the well known centers of strong convection over South America and central Africa. The high mixing ratios are present all year over equatorial Africa. There is some seasonal movement evident over South America, with moist air being found around Panama between May and September and over Brazil the rest of the time. These areas of Central and South America and equatorial Africa were observed by Soden and Fu (1995); to have maxima in convection and resulting maxima in UTH. Figure 8 shows MLS to be wetter over the Brazilian region and drier over Panama during northern winter, with the situation reversed in northern summer. This region was noted by Newell et al. (1997) to have a large semiannual variability.

Figure 9 shows a longitude–time section of the difference between equatorial mixing ratios from MLS and ECMWF (MLS − ECMWF). The longitude–time section was made using a distance-weighted interpolation onto grid points spaced every 5° in longitude around the equator (Clark et al. 1998). The position of the land and ocean is clearly reflected in this pattern. MLS is drier than ECMWF (the shaded regions) over the Indian Ocean, eastern Pacific, and Atlantic but is wetter than ECMWF in the more convectively active areas of the western Pacific and the landmasses of Africa and South America. In comparisons with Vaisala radiosondes (Read et al. 2001), MLS V490 was found to be too wet in dry regions and too dry in regions of high RHi. This result suggests that the real continent–ocean contrasts may be more extreme than either MLS or ECMWF indicate.

Semiannual variability can be seen over the Indian Ocean, South America, and the Atlantic Ocean. The

mismatch in water vapor concentration is particularly evident at 280°E, the edge of South America, from April to June and from September to November, during which period MLS indicates it to be 36 ppmv wetter than in ECMWF (hatched regions). At the same times, MLS shows the Indian Ocean to be drier than ECMWF. The difference is smaller during January–March and between August and September, which is reflected in the improved correlation coefficients seen in Fig. 4 at the same times. The mismatch of convection in this region has contributed greatly to the semiannual oscillation of the correlation coefficient in Fig. 4.

### *c. The Asian monsoon*

The Asian monsoon region shows some interesting differences between the two fields. The spatial extent of the moistening associated with the Asian monsoon in JJA is greater in the MLS observations than in the ERA data. During JJA, the high mixing ratios are located over India, Southeast Asia, and up to 30°N. A high moisture content remains in the Bay of Bengal until September and moves southeastward to Indonesia in October. Figure 8 shows the monsoon region to be drier in the ECMWF analyses except during June, for which month we know that MLS was experiencing some problems and there are few valid days in the monthly mean. The subsidence zones, which are located to the northwest (over the Arabian Peninsula) and southeast (over Australia) of the annual monsoon region, are much moister than is shown by MLS. During July, August, and September, the Arabian Peninsula was seen to have a low mixing ratio in MLS V490 data at 316, 215, and 147 hPa (Stone et al., 2000). High brightness temperatures, which reveal dry air, were observed with TOVS in this region (Wu et al. 1993), particularly in July. Although TOVS data have been assimilated into the ECMWF model, the Arabian Peninsula region is still observed to be drier by MLS, and it would seem that the ECMWF analyses fail to capture the moisture contrast between large-scale convective and subsidence areas.

## 5. Conclusions

In this paper we have analyzed water vapor from MLS, version 5, and from ECMWF. Such a comparison is useful since the MLS measurements are not used in the ECMWF assimilation. The conversion from RHi to mixing ratio highlights the sensitivity to the temperature fields used, with different temperature fields introducing different variability and different absolute values of mixing ratio. Using the same temperature fields for conversion means that the resulting mixing ratio fields are no longer totally independent of each other. Any differences between them, however, must then result from the water vapor measurements themselves.

To maximize confidence in the MLS measurements and to minimize the differences between the two fields stemming from their different horizontal and vertical resolutions, we prepared the fields for comparison in a number of steps. Although contamination by cirrus is expected to be small, we reset MLS RHi values greater than 120% back to 100%. We accounted for the difference in vertical resolution between the two datasets by multiplying vertical profiles of ECMWF RHi by the MLS averaging kernels. The yaw-cycle effect in MLS data was removed using a simple linear approximation to the antenna radiance change. The measurements were zonally averaged and were given an area weighting to try to account for the sampling difference between ECMWF and MLS.

Despite making these adjustments, there remain significant differences between the two fields. On a daily basis, spatial correlations between MLS and ECMWF are low (0.53) and exhibit a semiannual cycle, with the correlation coefficient improving during February and August when the ITCZ has its most extreme displacement from the equator. A longitude–time section showed there to be a semiannual disparity in moisture concentration over South America, with the maximum difference occurring from April to June and from September to November. The correlations during these periods were particularly low.

We have found that there is a lack of contrast between dry and moist areas, or areas of convection and subsidence. In comparison with ECMWF, MLS indicates greater moisture content in the air over convectively active regions and much drier air over oceanic areas and in areas which motion is expected to be downward, such as northwest and southeast of the Asian monsoon. This result is in agreement with other studies, and thus it would appear that the strength of global and regional circulations is not sufficiently well captured by ECMWF.

This paper illustrates the necessity for accurate global measurements of water vapor, and we await the completion of the ERA-40 analysis and the launch of the Earth Observing System Microwave Limb Sounder to enable a more comprehensive study of the variability of water vapor over longer timescales.

*Acknowledgments.* We thank Bill Read for many useful comments. This work was funded by NERC.

REFERENCES

Barath, F., and Coauthors, 1993: The Upper Atmosphere Research Satellite Microwave Limb Sounder instrument. *J. Geophys. Res.*, **98,** 10 751–10 762.

Bond, S., 1996: The potential effect of cirrus on microwave limb sounder retrievals. Ph.D thesis, University of Edinburgh, 99 pp.

Chandra, S., J. R. Ziemke, W. Min, and W. G. Read, 1998: Effects of 1997–1998 El Niño on tropospheric ozone and water vapor. *Geophys. Res. Lett.*, **25,** 3867–3870.

Clark, H. L., R. S. Harwood, P. W. Mote, and W. G. Read, 1998: Variability of water vapor in the tropical upper troposphere as

measured by the Microwave Limb Sounder on UARS. *J. Geophys. Res.*, **103,** 31 695–31 707.
Courtier, P., and Coauthors, 1998: The ECMWF implementation of three-dimensional variational assimilation (3D-Var). I: Formulation. *Quart. J. Roy. Meteor. Soc.*, **124,** 1783–1807.
Elliot, W. P., and D. J. Gaffen, 1991: On the utility of radiosonde humidity archives for climate studies. *Bull. Amer. Meteor. Soc.*, **72,** 1507–1520.
Elson, L. S., W. G. Read, J. W. Waters, P. W. Mote, J. S. Kinnersley, and R. S. Harwood, 1996: Space–time variations in water vapor as observed by the UARS Microwave Limb Sounder. *J. Geophys. Res.*, **101,** 9001–9015.
Eyre, J. R., G. Kelly, A. P. McNally, E. Andersson, and A. Persson, 1993: Assimilation of TOVS radiances through one-dimensional variational analysis. *Quart. J. Roy. Meteor. Soc.*, **119,** 1427–1463.
Gibson, J. K., P. Kallberg, S. Uppala, A. Hernandez, A. Nomura, and E. Serrano, 1997: ERA description. ECMWF Reanalysis Project Rep. Series, No. 1, 74 pp.
Knollenberg, R. G., K. Kelly, and J. C. Wilson, 1993: Measurements of high number densities of ice crystals in the tops of cumulonimbus. *J. Geophys. Res.*, **98,** 8639–8664.
Livesey, N. J., and Coauthors, 2002: The UARS Microwave Limb Sounder version 5 dataset: Theory, characterization, and validation. *J. Geophys. Res.*, in press.
McNally, A. P., and M. Vespirini, 1996: Variational analysis of humidity information from TOVS. *Quart. J. Roy. Meteor. Soc* **122,** 1521–1544.
Newell, R. E., Y. Zhu, W. G. Read, and J. W. Waters, 1997: Relationship between tropical upper tropospheric moisture and eastern tropical Pacific sea surface temperature at seasonal and interannual time scales. *Geophys. Res. Lett.*, **24,** 25–28.
Newman, M., P. D. Sardeshmukh, and J. W. Bergman, 2000: An assessment of the NCEP, NASA, and ECMWF reanalyses over the tropical west Pacific warm pool. *Bull. Amer. Meteor. Soc.*, **81,** 41–48.
Rabier, F., J-N. Thépaut, and P. Courtier, 1998: Extended assimilation and forecast experiments with a four-dimensional variational assimilation system. *Quart. J. Roy. Meteor. Soc.*, **124,** 1861–1887.
Read, W. G., J. W. Waters, D. A. Flower, L. Froidevaux, R. F. Jarnot, D. L. Hartmann, R. S. Harwood, and R. B. Rood, 1995: Upper-tropospheric water vapor from *UARS* MLS. *Bull. Amer. Meteor. Soc.*, **76,** 2381–2389.
——, and Coauthors, 2001: UARS MLS upper tropospheric humidity measurement: Method and validation. *J. Geophys. Res.*, **106,** 32 207–32 258.
Reber, C. A., 1993: The Upper Atmosphere Research Satellite (UARS). *Geophys. Res. Lett.*, **20,** 1215–1218.
Salathé, E. P., and D. Chesters, 1995: Variability of moisture in the upper troposphere as inferred from TOVS satellite observations and the ECMWF model analysis in 1989. *J. Climate*, **8,** 120–132.
Sandor, B. J., W. G. Read, J. W. Waters, and K. H. Rosenlof, 1998: Seasonal behavior of tropical to mid-latitude upper tropospheric water vapor from UARS MLS. *J. Geophys. Res.*, **103,** 25 935–25 947.
Schmetz, J., and O. M. Turpeinen, 1988: Estimation of the upper tropospheric humidity field from Meteosat water vapor image data. *J. Appl. Meteor.*, **27,** 889–899.
——, and L. van de Berg, 1994: Upper tropospheric humidity observations from Meteosat compared with short-term forecast fields. *Geophys. Res. Lett.*, **21,** 573–576.
Simmons, A. J., A. Untch, C. Jakob, P. Kallberg, and P. Unden, 1999: Stratospheric water vapor and the tropical tropopause temperatures in ECMWF analyses and multi-year simulations. *Quart. J. Roy. Meteor. Soc.*, **125,** 353–386.
Smith, W. L., H. M. Woolf, C. M. Hayden, D. Q. Wark, and L. M. McMillin, 1979: The TIROS-N Operational Vertical Sounder. *Bull. Amer. Meteor. Soc.*, **60,** 1177–1187.
Soden, B. J., and F. P. Bretherton, 1993: Upper-tropospheric relative humidity from the GOES 6.7 $\mu$m channel: Method and climatology for July 1987. *J. Geophys. Res.*, **98,** 16 669–16 688.
——, and ——, 1994: Evaluation of water vapor distribution in general circulation models using satellite observations. *J. Geophys. Res.*, **99,** 1187–1210.
——, and R. Fu, 1995: A satellite analysis of deep convection, upper tropospheric humidity and the greenhouse effect. *J. Climate*, **8,** 2333–2351.
——, and J. R. Lanzante, 1996: An assessment of satellite and radiosonde climatologies of upper-tropospheric water vapor. *J. Climate*, **9,** 1235–1250.
Stone, E. M., L. Pan, B. J. Sandor, W. G. Read, and J. W. Waters, 2000: Spatial distributions of upper tropospheric water vapor measurements from the UARS Microwave Limb Sounder. *J. Geophys. Res.*, **105,** 12 149–12 161.
Trenberth, K. E., D. P. Stepaniak, and J. W. Hurrell, 2001: The quality of reanalyses in the Tropics. *J. Climate*, **14,** 1499–1510.
van Loon, H., and R. L. Jenne, 1970: On the half-yearly oscillations in the tropics. *Tellus*, **22,** 391–398.
Vespirini, M., 1998: Humidity in the ECMWF model: Monitoring of operational analyses and forecasts using SSM/I observations. *Quart. J. Roy. Meteor. Soc.*, **124,** 1313–1327.
Vincent, D. G., 1994: The South Pacific convergence zone (SPCZ): A review. *Mon. Wea. Rev.*, **122,** 1949–1970.
Waters, J. W., 1993: Microwave limb sounding. *Atmospheric Remote Sensing by Microwave Radiometry*, M. A. Janssen, Ed., John Wiley and Sons, 383–496.
——, and Coauthors, 1999: The *UARS* and EOS Microwave Limb Sounder experiments. *J. Atmos. Sci.*, **56,** 194–218.
Wu, X., J. J. Bates, and S. J. Khalsa, 1993: A climatology of the water vapor brightness temperatures from NOAA operational satellites. *J. Climate*, **6,** 1282–1300.